Cambridge Centre for Computational Chemical Engineering

University of Cambridge

Department of Chemical Engineering

Preprint ISSN 1473 – 4273

Modelling soot formation in a premixed flame using an aromatic-site soot model and an improved oxidation rate

Matthew S Celnik, Markus Sander, Abhijeet Raj, Richard H West,

Markus Kraft*

released: 18 December 2007

Department of Chemical Engineering
Cambridge University
New Museums Site
Pembroke Street
Cambridge CB2 3RA
UK
*E-mail: mk306@cam.ac.uk

Preprint No. 53

c4e

Key words and phrases: soot, modelling, aromatic site, oxidation, DFT

Edited by
Cambridge Centre for Computational Chemical Engineering
Department of Chemical Engineering
University of Cambridge
Cambridge CB2 3RA
United Kingdom.

Fax: + 44 (0)1223 334796
E-Mail: c4e@cheng.cam.ac.uk
World Wide Web: http://www.cheng.cam.ac.uk/c4e/

Abstract

An updated rate of O_2 oxidation of one to four ring polyaromatic hydrocarbons in premixed flames is presented based on density function theory simulations of oxygen attack at different radical sites on various PAHs. The rate is in agreement with other rates found in the literature; however, it is several orders of magnitude lower than the currently accepted oxidation rate of multi-ring aromatic species, including soot. Simulations are presented of a premixed flame using this improved rate and a new advanced soot particle model, which is developed in this paper. This model includes unprecedented detail of the particles in the ensemble, including the aromatic content, C/H composition and primary-particle aggregate structure. The O_2 oxidation rate calculated in this paper is shown to give a better prediction of particle number density and soot volume fraction for a premixed flame. The predicted particle size distributions are shown also to describe better the experimental data. Predicted C/H ratio and PAH size distributions are shown for the flame. Computed TEM-style images are compared to experimental TEM images, which show that the aggregate structure of the particles is well predicted.

Contents

1 Introduction **5**

2 Estimating the rate of O_2 oxidation **6**

3 Aromatic-site (ARS) model **9**

4 Particle structure model **11**

5 Flame simulations **11**

6 Results **12**

6.1 Particle composition 15

6.2 Particle structure 17

7 Conclusions **18**

1 Introduction

Soot formation is an important process for industry and for the environment. It is generally acknowledged that polyaromatic hydrocarbons (PAHs) are the precursors to soot particles. This has been inferred from the essentially graphitic nature of nascent soot [13].

The soot model proposed by Frenklach and Wang [8], generally referred to as the ABF model, remains the basis for most soot models currently in use for premixed flames. The ABF model considers soot growth by addition of acetylene via the hydrogen-abstraction—carbon-addition (HACA) mechanism and by condensation of PAHs, though usually only pyrene is considered. Appel et al. [2] updated the model to include a correlation for active surface sites (alpha), which was fitted to data from a set of premixed flames. Alpha is an empirical correlation which accounts for the surface aging effect observed in sooting systems, and was formulated as a function of temperature and reduced particle mass.

The ABF model includes O_2 and OH oxidation of soot particles, however, the rates of these processes are questionable. The gas-phase mechanism of Wang and Frenklach [30] treats the rate of O_2 oxidation of one to four ring aromatic species as equal to the rate for phenyl. They also indicate that there are substantial uncertainties in the rate of phenyl oxidation. The ABF soot model also considers the rate of soot oxidation to be equal to the rate of phenyl oxidation [2], ignoring the affect that the neighbouring geometry on large aromatics might have. Oxidation is crucially important to combustion processes, and it is important that accurate rate expressions are available.

In order to capture all aspect of flame-generated soot, models must consider particle shape and structure as well as composition. Common shape models include spherical particles [8] and fractal models [16] which describe particles by two coordinates: size and a shape descriptor, for example surface area [23] or fractal dimension [16]. Recent studies using Monte-Carlo algorithms to solve sooting systems [21] have used very complex particle descriptions which account for the relative positions of each primary particle within an aggregate. Such models enable 3D images of aggregates to be generated, however, they are very computationally expensive.

Until recently soot particle models have been necessarily simple in order to allow particle ensembles to be simulated in computationally reasonable timescales. Often particles are considered to consist of uniformly graphitic carbon only [3], and simple spherical or surface-volume shape models have been used. Often these restrictions are imposed by the numerical technique used. Moment methods [7] are very fast but are restricted to a one or two dimensional particle spaces, as the number of moment equations scales exponentially with the number of particle coordinates. They also allow no resolution of the particle size distribution (PSD) without a further assumption about its shape. Sectional techniques [31] can also be fast and allow the PSD to be resolved, however they can suffer from numerical diffusion [22] and they also do not scale favourably with the size of the particle state space. Monte-Carlo methods [3] are generally slower than other techniques and have only been coupled to simple systems [5], however, they allow very detailed particle descriptions to be used, such as the model discussed in this paper.

Recently kinetic Monte-Carlo (KMC) and molecular dynamics (MD) [29, 9] have been used to study the growth of single PAH molecules and graphene sheets. These techniques

allow very complex particles to be modelled, however, the high computational expense make it currently prohibitive to use these techniques to model entire particle ensembles.

The purpose of this paper is to present updated O_2 oxidation rates for small aromatics and soot particles. These rates are incorporated into a new soot particle model for premixed laminar flames. This model consists of two sub-models which have been considered separately in the past. The first sub-model describes soot particles by their aromatic structure [6], and has previously been applied to soot formation in a plug-flow reactor. The second sub-model uses a primary particle list to describe aggregate structure, which allows TEM-style images to be generated and directly compared to experimentally obtained TEMs [32].

2 Estimating the rate of O_2 oxidation

Only oxidation processes involving one free-radical carbon atom are investigated here. Oxidation reactions on repeating zig-zag and armchair edges with multiple neighbouring radical sites have already been investigated by Sendt and Haynes [25, 26].

At high temperatures the reaction between a free radical site on a graphene ring and an oxygen molecule occurs mainly through the metathetical process [20]:

$$C^{\bullet} + O_2 \rightarrow C\text{–}O + O \tag{1}$$

$C^{\bullet}$ represents a radical site on a PAH. The bond between the oxygen atoms is broken and one atom connects to the free radical site while the other atom remains in the surrounding gas and can undergo further reactions. This is assumed to be the rate-limiting step for PAH oxidation [30].

Oxidation rates of benzene, naphthalene, anthracene, phenanthrene, pyrene and benzo[a]anthracene at different carbon atoms have been calculated to allow the dependence of the oxidation rate on the radical site geometry to be studied. Oxidation processes were investigated using density functional theory (DFT) at a B3LYP/6-31G(d) level of theory. Kunioshi et al. [19] have previously investigated the oxidation rate of phenyl, naphthyl and pyrenyl, and concluded that the rate is independent of the number of carbon rings. The purpose of this work is to investigate the dependence of the oxidation reaction on the neighbouring geometry. Fig. 1 shows the transition states studied, in addition to those calculated by Kunioshi et al.

All quantum mechanical calculations were performed using the GAMESS-UK program suite [11]. The structures of the reactants and the transition states have been optimized, and the vibrational frequencies calculated to verify that the stable species have no imaginary frequencies, and that the transition states have exactly one imaginary frequency. The reaction pathway for anthracene can be seen in figure 2.

The temperature dependent oxidation rates were calculated in the range 700-3000 K using

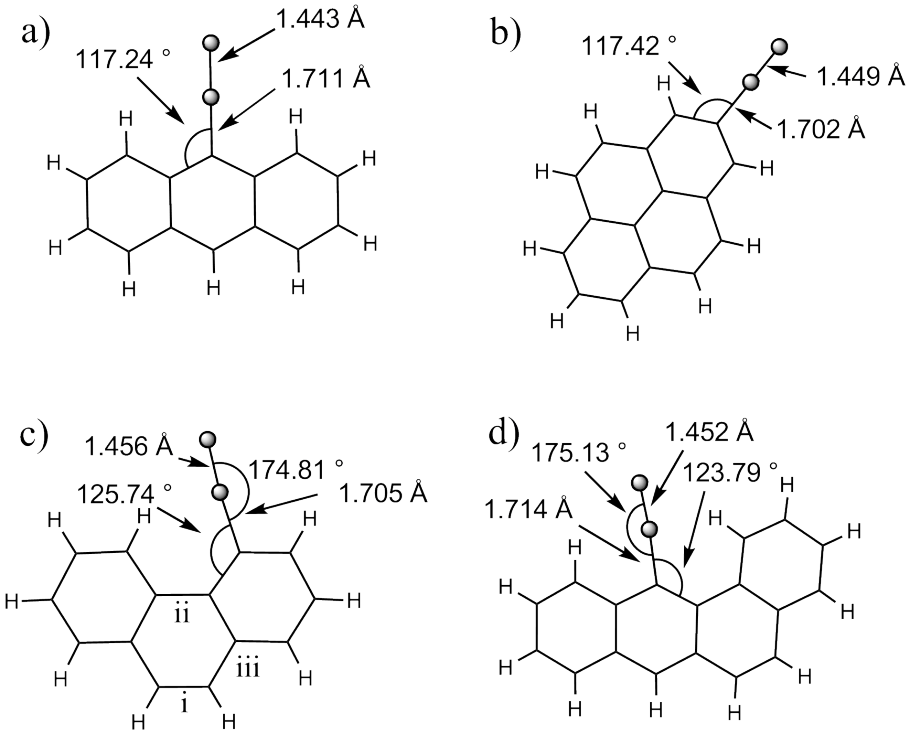

Figure 1: *Studied transition states for (a) anthracene, (b) C_2 pyrene, (c) phenanthrene and (d) benzo[a]anthracene. Labelled sites are (i) free-edge site, (ii) armchair site, (iii) zig-zag site.*

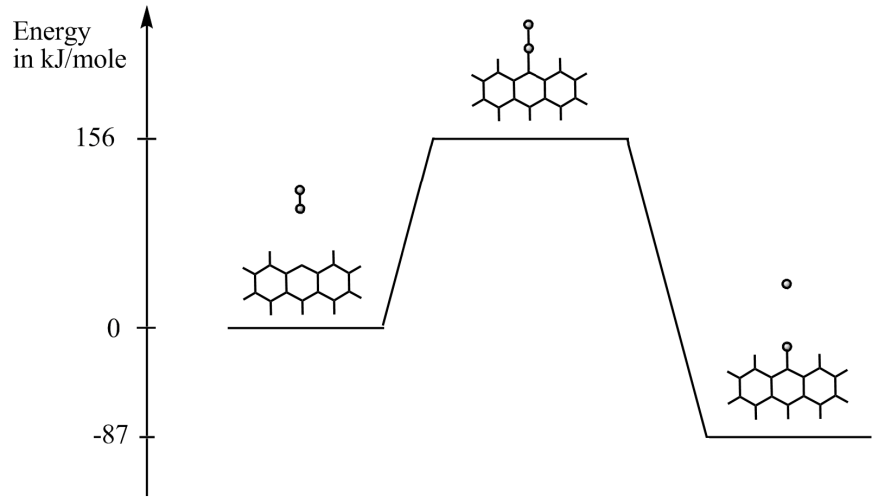

Figure 2: *Reaction pathway for anthracene.*

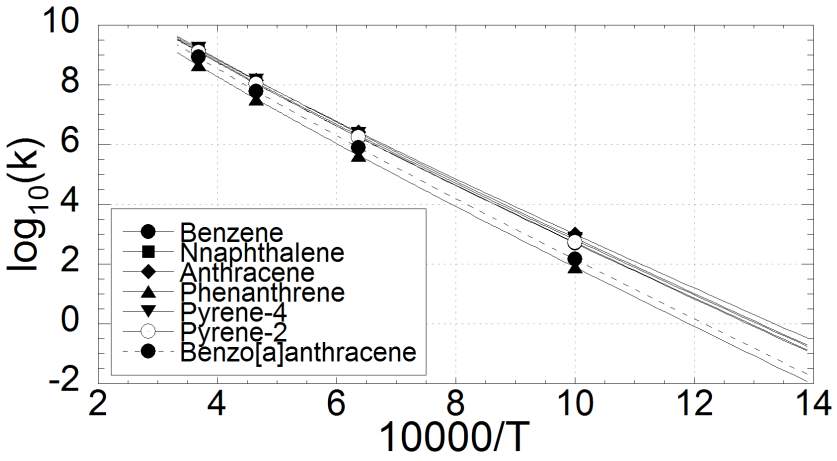

Figure 3: *O_2 oxidation rates as function of temperature for all studied PAH molecules. k in cm^3/mol s, T in K*

transition state theory (TST):

$$k(T) = \frac{k_B T}{h} \frac{Q^{\neq}}{Q_A Q_B} exp\left(\frac{-\Delta E}{k_B T}\right) \tag{2}$$

$Q^{\neq}, Q_A, Q_B$ are the total partition functions of the transition state and the reactants and ΔE is the activation energy. Tunnelling processes have been neglected in these calculations.

Fig. 3 shows the temperature dependence of the oxidation rate for all the studied molecules. A linear least-square fitting algorithm was used to calculate the Arrhenius rate coefficients using the expression:

$$k(T) = AT^n exp\left(\frac{-\Delta E}{RT}\right) \tag{3}$$

where T is the temperature in Kelvin. The calculated Arrhenius coefficients are given in table 1.

The calculated activation energies for benzene, naphthalene and pyrene oxidation agree with the energies calculated by Kunioshi et al. [19], suggesting that the energies calculated for the other molecules are also reasonable. For molecules where the oxidized carbon atom belongs to an armchair site (phenanthrene and Benzo[a]anthracene) the oxygen molecule the C-O-O angles are about $175°$ in both cases, and the C-C-O angles are $125.8°$ and $123.8°$ respectively, this induces an activation energy of 173 kJ/mol compared to about 160 kJ/mol for species where the oxygen molecule remains straight and the C-C-O angle is $117°$. This suggests that the change of the geometry induced by the Hydrogen atom on Carbon 4 (Anthracene) respectively Carbon 5 and 7 (Benzo[a]anthracene) is responsible for the higher activation energy. Fig. 3 shows that the difference of the oxidation rates for geometries where oxygen remains straight is negligible, whereas the higher activation en-

Table 1: *Arrhenius parameters for O_2 oxidation of one to five ring aromatics. A in (cm^3/mol s), ΔE in (kJ/mol).*

Molecule	A	n	ΔE
Benzene	7.7×10^3	2.43	162
Naphthalene	8.9×10^3	2.40	160
Anthracene	7.3×10^3	2.42	156
Phenanthrene	4.0×10^3	2.44	173
Pyrene-4	9.7×10^3	2.42	161
Pyrene-2	8.0×10^3	2.42	161
Benzo[a]anthracene	6.0×10^3	2.46	173

ergy for armchair oxidation leads to a lower rate. The oxidation rates for an armchair next to a zigzag (Benzo[a]anthracene) is higher than the rate for an armchair next to a free-edge site (phenanthrene) but still lower than the rates where the oxygen remains straight. A second transition state for the Benzo[a]anthracene oxidation process with an angle of $21.5°$ between the oxygen molecule and the plane in which the PAH structure is located has been found, but this transition state gives a lower reaction rate.

Jung et al. [15] investigated the oxidation process for soot particles at low temperatures experimentally and found an activation energy of 148 kJ/mol, which is in reasonable agreement with the activation energies reported here.

3 Aromatic-site (ARS) model

The previously reported ARS model [6] describes the aromatic content of soot particles by considering the different possible sites on aromatic structures. Four principal sites were identified and are shown in fig. 4. These are defined by the number of carbon atoms required to construct them: free-edges have two atoms, zig-zags have three atoms, armchairs have four atoms and bays have five atoms. Six atoms in a loop are assumed to rapidly form a new aromatic ring, so are neglected at present. This assumption will have to be tested in the future.

Additionally, the presence of 5-member rings on zig-zag sites has been suggested [9], therefore these are included in the model; however, 5-member rings in the graphite lattice are not considered. By neglecting the relative positions of the surface sites, it is possible to describe a soot particle by nine variables: carbon atom (C) and hydrogen atom (H) counts, the particle surface area (S_a), the number of edges (N_{ed}), zig-zags (N_{zz}), armchairs (N_{ac}), bays (N_{bay}), 5-member rings (N_{R5}) and the number of PAHs (N_{PAH}). Therefore, particles are described by a nine dimensional type:

$$X = (C, H, S_a, N_{ed}, N_{zz}, N_{ac}, N_{bay}, N_{R5}, N_{PAH}) \tag{4}$$

This model is referred to as the site-counting model [6]. The motivation for neglecting the relative site positions is to maintain as much information about the soot PAH structure as

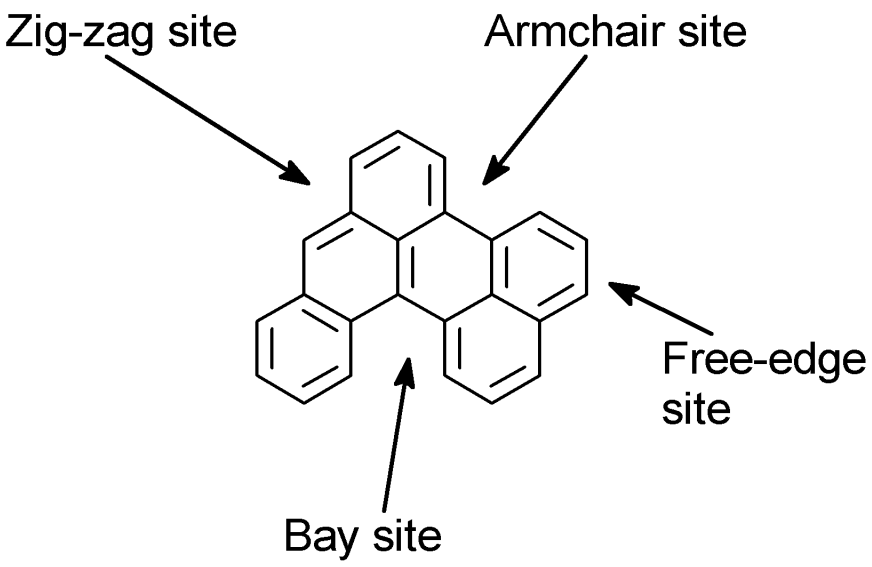

Figure 4: *An example PAH structure showing the four principal site types.*

possible, while keeping the computational expense low enough to simulate large particle ensembles, rather than just single particles.

Some surface processes require more than one site to be contiguous on the PAH edge, for example a 6-member ring can be considered as three consecutive free-edges. As no positional information is stored, correlations for such combined-sites have been developed by Raj et al. [24] which provide the number of these combined-sites in terms of the principal sites.

Surface processes necessarily change the structure of the PAH surface. Simple geometric considerations require that each surface site has two neighbouring sites. These neighbouring sites must be updated when a process is simulated. In general, ring addition will increase the number of carbon atoms in each neighbour by one, thereby moving the site type up the chain: free-edge → zig-zag → armchair → bay. Ring desorption will reduced the number of carbons in each neighbouring site by one, thereby moving the site type down the chain. Not all site types are equally likely to neighbour other sites, hence a set of process-dependent site weights are used to select neighbouring sites depending on the process being simulated. These are also given by Raj et al. [24], who used a KMC algorithm to simulate single PAH molecules using the same surface processes as the site-counting model.

The complex, multi-dimensional particle state space of the site-counting model demands a solution technique such as a Monte-Carlo particle method to be computationally tractable. Soot particle growth is therefore modelled as a stochastic process where the data set is an ensemble of computational particles [3] with the properties defined above. The stochastic jump processes are calculated using the set of soot surface reactions detailed by Celnik et al. [6]. The reader is referred to that reference for a detailed analysis of the surface processes. Ring growth by acetylene and ring desorption processes are included, based

on the work of Frenklach et al. [9], as well as oxidation processes at both free-edges and armchairs, using the rates presented in this paper. The jump-process rates were calculated by assuming steady-state of the short-lived intermediates.

4 Particle structure model

In order to describe the aggregate structure of the soot particles, the primary-particle tracking algorithm of West et al. [32] was used. A list of primary particles (hereafter, primaries) is maintained independently for each soot particle (hereafter, aggregate). The assumptions that the primaries are spherical and have uniform density are made, therefore each primary is fully described by the number of C atoms it contains. At particle inception an aggregate is assumed to be spherical and is assigned one primary. On coagulation the list of primaries of both aggregates are appended. The surface-volume model [23] is formulated such that all surface processes increase aggregate sphericity, and hence decrease specific surface area. Each aggregate's primaries are regularly updated such that the combined primary surface area matches that predicted by the surface-volume model. This is modelled by removing primaries, starting with the smallest, and redistributing the C atoms across the remaining primaries, weighted by their surface area. This is repeated until the primary surface area is less than or equal to the surface-volume surface area. This mimics the situation in which smaller primaries are subsumed into larger ones due to surface growth. Each aggregate is therefore described by a vector of primaries (P) of length N_{pri}, hence the particle type now has a minimum of ten dimensions ($N_{pri} + 9$):

$$X_p = \left(X, P_{1,2\ldots N_{pri}}\right) \tag{5}$$

In the current simulations, typical values of N_{pri} were observed in the range 5-20, which gives a particle type of 14-29 variables.

The aromatic-site-counting—primary-particle model, which combines the above descriptions of particle composition and structure, shall be referred to as the ARSC-PP model.

5 Flame simulations

The model presented here is very detailed and capable of predicting a large number of features of sooting systems, therefore the premixed flames of Abid et al. [1] were used for comparison, as experimentally obtained data were available for particle number density, soot volume fraction and particle size distributions, as well as TEM images. The premixed flame chemistry was solved using the PREMIX code [17], including a method-of-moments approximation for soot formation [7]. The Monte-Carlo particle solver was then run as a post-processing step [3] using the ARSC-PP model. Computations are presented only for the flame designated HWC4 (C4 in [1]) here, though similar results have been observed for the other flames, C1-C5, presented in that paper.

The gas-phase combustion mechanism of Wang and Frenklach [30], updated by Appel

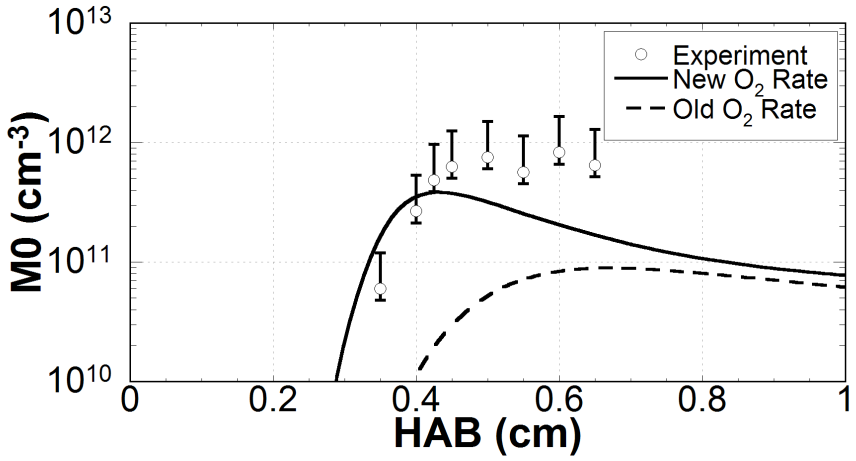

Figure 5: *Particle number density as a function of height above burner. HAB shifted by +0.15 cm.*

et al. [2] was used to model the gas-phase chemistry. This mechanism includes the formation of aromatic species up to pyrene. The gas-phase mechanism was modified to include the new aromatic O_2 oxidation rate detailed in this paper for two, three and four ring PAHs (naphthalene, anthracene and pyrene respectively). The O_2 oxidation rate for pyrene-4 was used as the rate for soot particles in the ARS soot mechanism. The rate of O_2 oxidation presented here is much lower than the current ABF value, therefore it is expected that a greater quantity of soot should be predicted.

6 Results

Fig. 5 shows the comparison of the ARSC-PP model to the experimentally observed particle number density (M0). The simulations underpredict the experimental M0 using both oxidation rates. The new oxidation rates show reasonable agreement during the inception phase, however, they appear to underpredict M0 at later stages. The ABF oxidation rate severely underpredicts M0 at all heights above burner (HAB). Abid et al. [1] discuss how the SMPS probe delays the formation of soot, and they "shift" their data by -0.35 cm (upstream) to account for this. It was found that the simulations presented here better matched the experimental data if the results were shifted back 0.15 cm (downstream). This seems valid as the exact retardation of soot formation due to the SMPS probe is not exactly known, and the shifted position lies in between the actual and shifted positions reported by Abid et al..

Fig. 6 shows the comparison of the ARSC-PP model to the experimentally observed soot volume fraction (Fv). Again the results have been shifted by 0.15 cm downstream. Both simulations underpredict Fv by more than one order of magnitude, even when considering the confidence intervals due to the uncertainty in the measured temperature profiles, however, this is an acceptable result for soot prediction [4]. The improved oxidation rate shows a substantial increase in Fv over the original rate, which demonstrates that it is

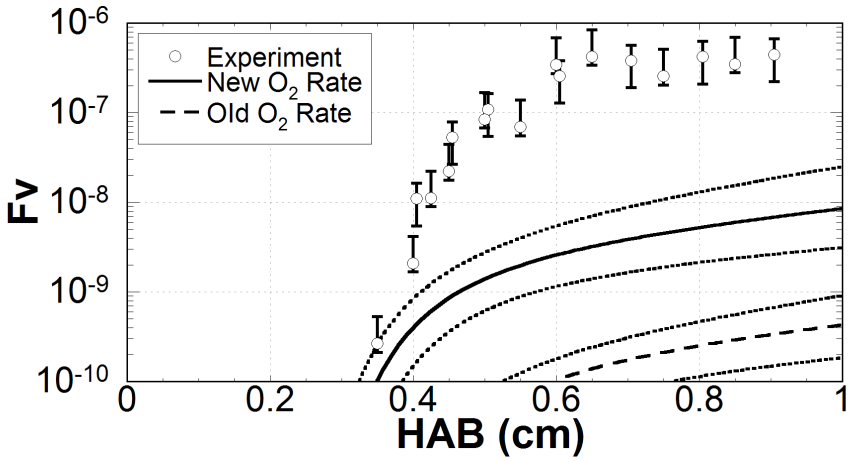

Figure 6: *Soot volume fraction as a function of height above burner. Short-dashed lines indicate confidence intervals due to the 50 K uncertainty in the experimentally measured flame temperature. HAB shifted by +0.15 cm.*

more appropriate in this case. There is also some uncertainty about the soot density assumed by Abid et al. [1], which might account for some of the discrepancy between the simulations and the experiments.

Fig. 7 shows the comparison of the ARSC-PP model to the experimentally obtained particle size distributions (PSDs). The PSDs were calculated using the kernel density estimation (density) function of the statistical package R [10] with a bandwidth of 0.03$\times$d, where d is the aggregate collision diameter [23]. The ABF oxidation rate underpredicts the particle sizes at all HABs. In general, the improved oxidation rates give a much more appropriate fit to the experimental data. At the first HAB = 0.5 cm the simulation already predicts bimodality, which is not observed in the experimental data. At HAB = 0.6 cm there is good agreement for the larger particles, however the trough is predicted to occur at a lower diameter (2.5 nm instead of 6 nm), also the number of particles in that range are underpredicted. This result is consistent with the findings of Singh et al. [27], who demonstrated that the trough position can be better predicted if the size of the incepting PAH molecule is increased. This trend continues at HAB = 0.8 cm, although the simulation now underpredicts the peak diameter and the number of larger particles. The trough depth, however, is better matched. At the last observed point, HAB = 1.0 cm, there is a severe underprediction of the largest particles, although the trough at around 4-4.5 nm is beginning to match the experimental data better than at other points. In general, the simulations are able to capture the qualitative properties of the experimental data, including the onset of bimodality, and are reasonably good at predicting the quantitative properties also. The disagreement at larger particle sizes is probably a symptom of the underprediction of Fv (fig. 6).

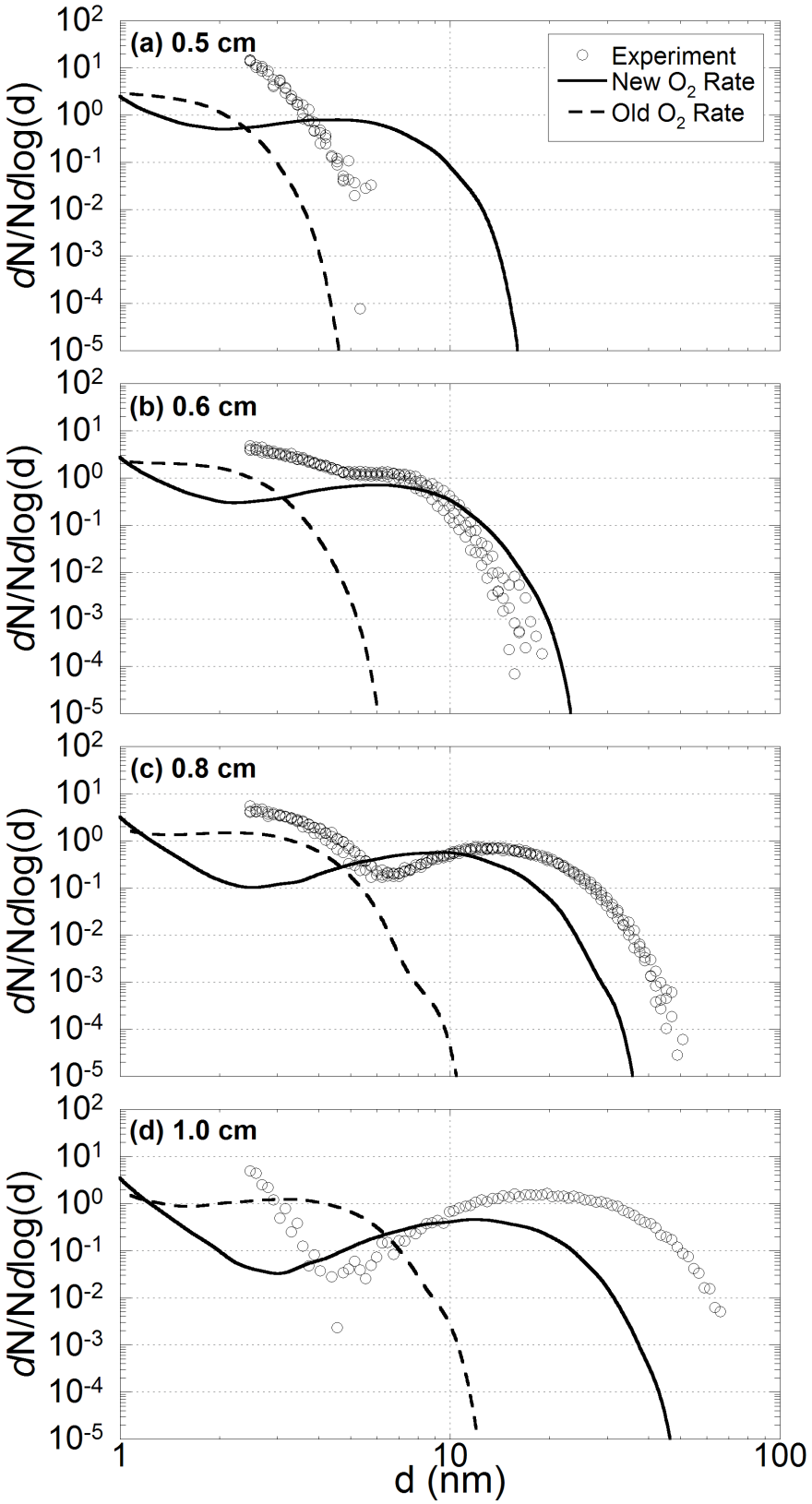

Figure 7: *Particle size distributions at different heights above burner (shifted by +0.15 cm).*

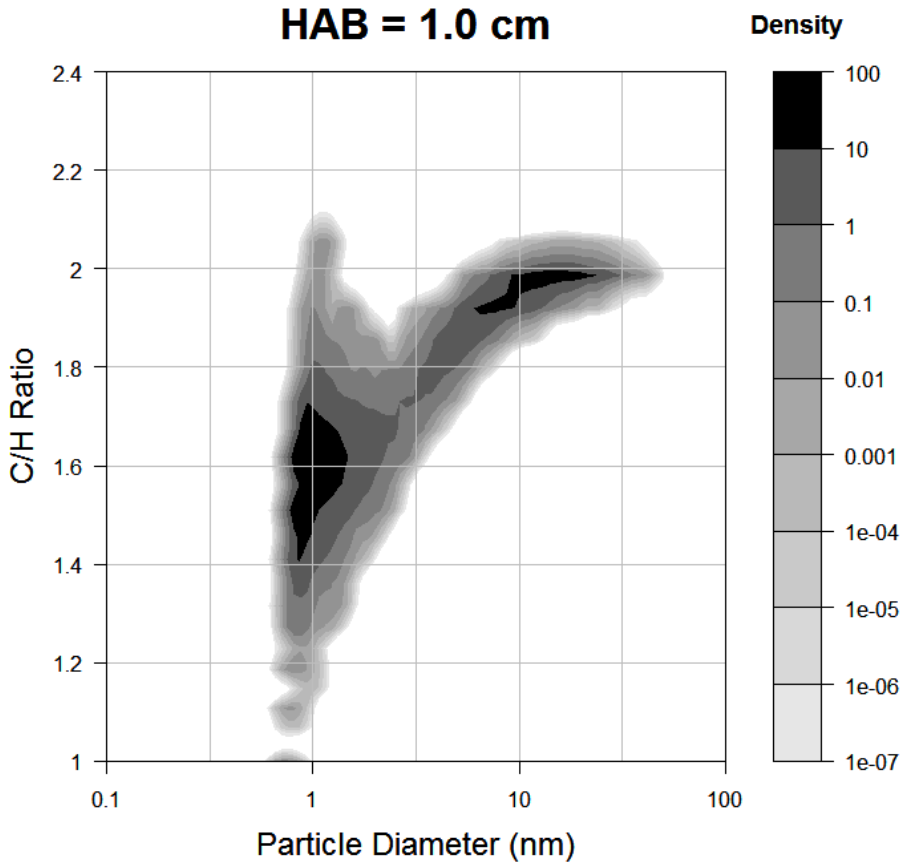

Figure 8: *Particle C/H Ratio density plot against particle diameter at HAB = 1.0 cm.*

6.1 Particle composition

Fig. 8 shows the particle C/H ratio distribution against particle diameter at HAB = 1.0 cm. The 2D kernel density estimation (kde2d) function of R was used to calculate the distribution, using 100 points in each direction. The bimodality of the particle distribution can be clearly seen. The left-most density maximum occurs around C/H = 1.6, which is equivalent to pyrene ($C_{16}H_{10}$). This is an artefact of the soot inception model used, which assumes that the dimerisation of pyrene is the only route of particle formation, so in this respect the result is uninteresting. The second peak occurs at C/H values around 2, which is consistent with reported values for young soot particles [29]. It is interesting that there is little variation of the C/H ratio for particles between 10-40 nm, in fact the C/H ratio appears to converge on a value just below 2. Far higher ratios are presented in the literature, for example Harris and Weiner [12] report about 7 and Homann [14] reports about 10. It has been suggested [6] that a process such as graphitisation could be responsible for such an increase in C/H ratio, but this has not been considered here.

Fig. 9 shows the approximate average sub-particle PAH ring count distribution against particle diameter at HAB = 1.0 cm. The distribution was calculated using R in the same

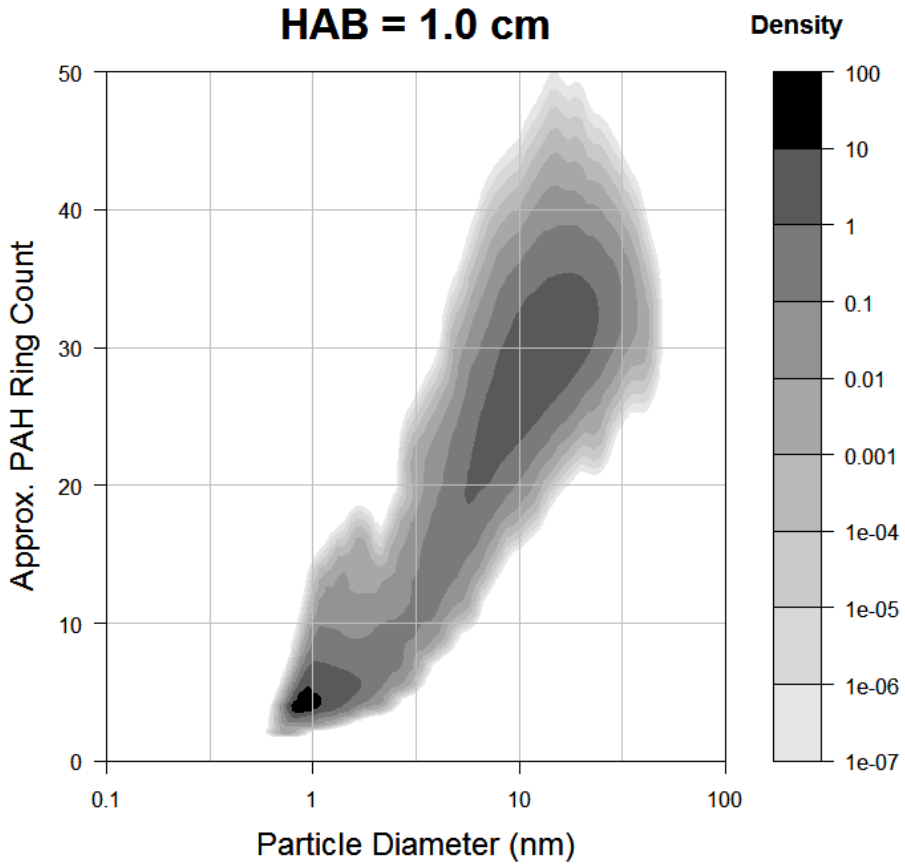

Figure 9: *Approximate average sub-particle PAH ring counts calculated assuming a square PAH arrangement.*

manner as the C/H ratio. The ring counts were calculated assuming that the PAH had a m×m ring arrangement, such that the number of rings (N_{rng}) is given by eqn. 6:

$$N_{rng} = \left\lfloor \left(0.5\sqrt{(2 \times C/N_{PAH}) + 4} - 1\right)^2 \right\rfloor \tag{6}$$

Again the bimodality can be observed in this figure. The bottom left density peak corresponds again to pyrene (four rings). As the particle grow, the average size of the PAHs also increases. The ring counts in the range 4-40 correspond approximately to characteristic lengths of 0.5-2 nm, or 16-100 carbon atoms. These values compare favourably to the results of Vander Wal and Tomasek [28], though they report a few lengths up to 6 nm, which would correspond to a very large graphene structure for very compact PAHs, or a more open or linear arrangement of the PAH rings. In the first instance it is assumed here that the distribution of average PAH sizes over the ensemble should be representative of the distribution of PAH sizes within a large soot particle. This could be tested with future models. A future, more complex model is suggested to track each PAH in each particle individually, in order to generate per-particle PAH size distributions.

6.2 Particle structure

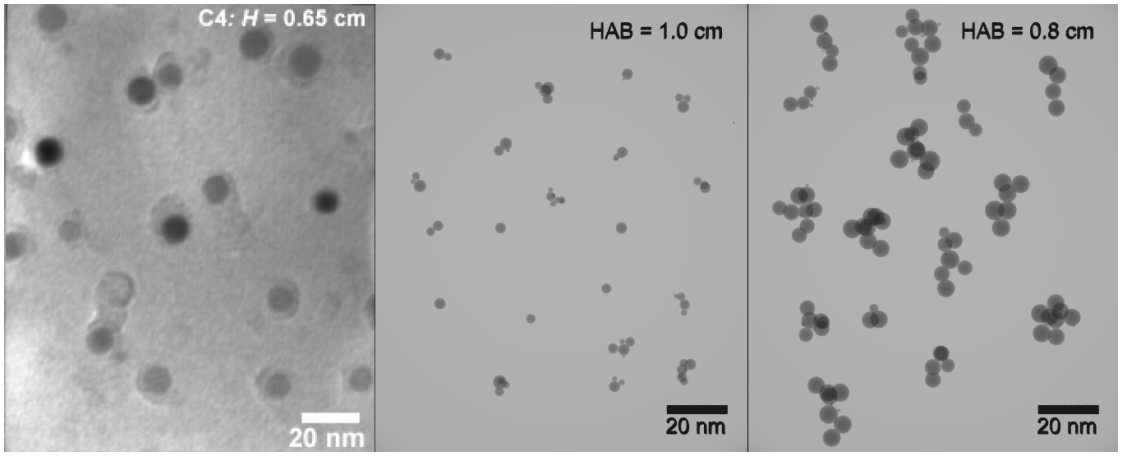

Figure 10: *Comparison of experimentally obtained TEM images with computationally generated images. Left panel is experimental TEM reproduced from Abid et al. [1]. Centre panel is a computationally generated TEM-style image using the old oxidation rate. Right panel is a computationally generated TEM-style image using the new oxidation rate.*

Fig. 10 shows computationally generated TEM-style images compared to experimentally obtained images. These TEM-style images were obtained by taking a selection of particles from the predicted ensemble and placing them on a grid of identical size to the experimental TEM. The centre panel demonstrates that the ABF oxidation rate generates small aggregates with diameters 5-10 nm. These do not compare well to the experimental image, which shows nearly-spherical primary particles around 10 nm in diameter, and possibly some evidence of aggregation on a larger scale. Abid et al. [1] argued that the captured particles must be liquid-like due to the apparent halos around the particles. They used AFM analysis to strengthen this argument. In this case the particles should be smaller than they appear on the grid, as they would have spread. However, the particles predicted using the old oxidation rate still appear too small for this to explain the discrepancy. The right-hand panel shows particles generated with the improved oxidation rates. Large aggregates are observed with diameters about 10-20 nm, and primary particle sizes around 5-10 nm. These particles compare more favourably in terms of size with those observed experimentally, however, the degree of aggregation predicted is not observed experimentally. A possible reason for this discrepancy is the surface-volume model assumption of aggregation, even for the smallest particles, as is observed in the centre panel. If the small particles are indeed liquid-like, then this assumption would be invalid. It may be necessary to include a size-dependent model for particle coalescence for small particles, which becomes inactive for larger particles [18]. This should slightly reduce the overall particle sizes, but should also reduce the predicted degree of aggregation.

7 Conclusions

New O_2 oxidation rates for two to four ring aromatics and soot have been presented based on quantum-chemistry calculations. The new rates are substantially lower than the previously accepted rate, which leads to enhanced soot production in flames. It has been shown that the oxidation rates are similar for all studied radical sites, except for those on an armchair. Armchair radical sites exhibit a higher activation energy, which was attributed to the need for the oxygen molecule to bend.

The soot particle model presented here is a step change for soot modelling. The combined aromatic-site-counting—primary-particle model allows a very detailed prediction of soot particle ensembles, including composition and aggregate structure. The model does not include any fitted parameters for surface chemistry, which were required in previous models. The model demonstrates reasonable agreement when compared to experimental observations of a premixed flame, although it still underpredicts soot volume fraction. Predictions of particle C/H ratio and constituent PAH size have been shown which agree well with reported values for young soot, although they are smaller than other values reported for flames. Graphitisation has been suggested as a process which could explain this. Finally, TEM-style images have been generated using the primary-particle model and compared to an experimentally obtained TEM image. The improved oxidation rates are shown to give better predictions of particle size, but the degree of aggregation is perhaps overpredicted.

References

[1] A D Abid, N Heinz, E D Tolmachoff, D J Phares, and H Wang. Relation between particle size distribution function and morphology of soot formed in atmospheric-pressure, premixed ethylene-oxygen-argon flame. In *5th US Combustion Meeting Papers*. Western States Section of the Combustion Institute, March 2007. Paper # F11.

[2] Jörg Appel, Henning Bockhorn, and Michael Frenklach. Kinetic modeling of soot formation with detailed chemistry and physics: Laminar premixed flames of C_2 hydrocarbons. *Combust. Flame*, 121:122–136, 2000. doi:10.1016/S0010-2180(99)00135-2.

[3] M Balthasar and M Kraft. A stochastic approach to solve the particle size distribution function of soot particles in laminar premixed flames. *Combust. Flame*, 133:289–298, 2003. doi:10.1016/S0010-2180(03)00003-8.

[4] M Balthasar, F Mauss, and H Wang. A computational study of the thermal ionization of soot particles and its effect on their growth in laminar premixed flames. *Combust. Flame*, 129:204–216, 2002. doi:10.1016/S0010-2180(02)00344-9.

[5] Matthew S Celnik, Robert I A Patterson, Markus Kraft, and Wolfgang Wagner. Coupling a stochastic soot population balance to gas-phase chemistry using operator splitting. *Combust. Flame*, 148(3):158–176, 2007. doi:10.1016/j.combustflame.2006.10.007.

[6] Matthew S Celnik, Abhijeet Raj, Richard H West, Robert I A Patterson, and Markus Kraft. An aromatic site description of soot particles. Technical Report 51, c4e Preprint-Series, Cambridge, 2007. URL http://como.cheng.cam.ac.uk.

[7] Michael Frenklach. Method of moments with interpolative closure. *Chem. Eng. Sci*, 57:2229–2239, 2002. doi:10.1016/S0009-2509(02)00113-6.

[8] Michael Frenklach and Hai Wang. Detailed modeling of soot particle nucleation and growth. *Proc. Combust. Inst.*, 23:1559–1566, 1990. doi:10.1016/S0082-0784(06)80426-1.

[9] Michael Frenklach, Charles A Schuetz, and Jonathan Ping. Migration mechanism of aromatic-edge growth. *Proc. Combust. Inst.*, 30:1389–1396, 2005. doi:10.1016/j.proci.2004.07.048.

[10] Robert Gentleman and Ross Ihaka. R statistical software, 2005. URL www.r-project.org. version 2.4.0.

[11] M.F. Guest, I. J. Bush, H.J.J. van Dam, P. Sherwood, J.M.H. Thomas, J.H. van Lenthe, R.W.A Havenith, and J. Kendrick. The GAMESS-UK electronic structure package: algorithms, developments and applications. *Mol. Phys.*, 103(6–8): 719–747, 2005. URL http://www.cfs.dl.ac.uk/gamess-uk/index.shtml.

[12] Stephen J Harris and Anita M Weiner. Chemical kinetics of soot particle growth. *Ann. Rev. Phys. Chem.*, 36:31–52, 1985. doi:10.1146/annurev.pc.36.100185.000335.

[13] B S Haynes and H Gg Wagner. Soot formation. *Prog. Energy Combust. Sci.*, 7(4): 229–273, 1981. doi:10.1016/0360-1285(81)90001-0.

[14] K H Homann. Carbon formation in premixed flames. *Combust. Flame*, 11(4):265–287, 1967. doi:10.1016/0010-2180(67)90017-X.

[15] Heejung Jung, David B Kittelson, and Michael R Zachariah. Kinetics and visualization of soot oxidation using transmission electron microscopy. *Combustion and Flame*, 136:445–456, 2004. doi:10.1016/j.combustflame.2003.10.013.

[16] A Kazakov and M Frenklach. Dynamic modeling of soot particle coagulation and aggregation: Implementation with the method of moments and application to high-pressure laminar premixed flames. *Combust. Flame*, 114:484–501, 1998. doi:10.1016/S0010-2180(97)00322-2.

[17] J Kee, K Grcar, M D Smooke, and J A Miller. Premix: A fortran program for modelling steady laminar one-dimensional premixed flames. Technical report, SANDIA National Laboratories, 1985.

[18] F Einar Kruis, Karl A Kusters, Sotiris E Pratsinis, and Brian Scarlett. A simple model for the evolution of the characteristics of aggregate particles undergoing coagulation and sintering. *Aerosol. Sci. Tech.*, 19(4):514–526, 1993. doi:10.1080/02786829308959656.

[19] Nilson Kunioshi, Minoru Touda, and Seishiro Fukutani. Computational study on the formation of five-membered rings in PAH through reaction with O_2. *Combustion and Flame*, 128:292–300, 2002. doi:10.1016/S0010-2180(01)00353-4.

[20] A M Mebel and M C Lin. Ab initio molecular orbital calculations of $C_6H_5O_2$ isomers. *J. Am. Chem. Soc*, 116(21):9577–9584, 1994. doi:10.1021/ja00100a023.

[21] Neal Morgan, Markus Kraft, Michael Balthasar, David Wong, Michael Frenklach, and Pablo Mitchell. Numerical simulations of soot aggregation in premixed laminar flames. *Proc. Combust. Inst.*, 31:693–700, 2007. doi:10.1016/j.proci.2006.08.021.

[22] S H Park, S N Rogak, W K Bushe, J Z Wen, and M J Thomson. An aerosol model to predict size and structure of soot particles. *Combust. Theor. Model.*, 9(3):499–513, 2005. doi:10.1080/13647830500195005.

[23] Robert I A Patterson and Markus Kraft. Models for the aggregate structure of soot particles. *Combust. Flame*, 151:160–172, 2007. doi:10.1016/j.combustflame.2007.04.012.

[24] Abhijeet Raj, Matthew S Celnik, Robert I A Patterson, Richard H West, and Markus Kraft. A statistical approach to develop a detailed soot growth model using PAH characteristics. Technical Report 52, c4e Preprint-Series, Cambridge, 2007. URL `http://como.cheng.cam.ac.uk`.

[25] Karina Sendt and Brian S Haynes. Density functional study of the chemisorption of O_2 on the armchair surface of graphite. *Proceedings of the Combustion Institute*, 30: 2141–2149, 2005. doi:10.1016/j.proci.2004.08.064.

[26] Karina Sendt and Brian S Haynes. Density functional study of the chemisorption of O_2 on the zig-zag surface of graphite. *Combustion and Flame*, 143:629–643, 2005. doi:10.1016/j.combustflame.2005.08.026.

[27] Jasdeep Singh, Robert I A Patterson, Markus Kraft, and Hai Wang. Numerical simulation and sensitivity analysis of detailed soot particle size distribution in laminar premixed ethylene flames. *Combust. Flame*, 145:117–127, 2006. doi:10.1016/j.combustflame.2005.11.003.

[28] Randall L Vander Wal and Aaron J Tomasek. Soot oxidation: dependence upon initial nanostructure. *Combust. Flame*, 134:1–9, 2003. doi:10.1016/S0010-2180(03)00084-1.

[29] Angela Violi. Modeling of soot particle inception in aromatic and aliphatic premixed flames. *Combust. Flame*, 139:279–287, 2004. doi:10.1016/j.combustflame.2004.08.013.

[30] Hai Wang and Michael Frenklach. A detailed kinetic modeling study of aromatic formation in laminar premixed acetylene and ethylene flames. *Combust. Flame*, 110: 173–221, 1997. doi:10.1016/S0010-2180(97)00068-0.

[31] John Z Wen, M J Thomson, S H Park, S N Rogak, and M F Lightstone. Study of soot growth in a plug flow reactor using a moving sectional model. *Proc. Combust. Inst.*, 30(1):1477–1484, 2005. doi:10.1016/j.proci.2004.08.178.

[32] Richard H West, Matthew S Celnik, Oliver R Inderwildi, Markus Kraft, Gregory J O Beran, and William H Green. Towards a comprehensive model of the synthesis of TiO_2 particles from $TiCl_4$. *Ind. Eng. Chem. Res.*, 46(19):6147–6156, 2007. doi:10.1021/ie0706414.